Journal of Organometallic Chemistry 881 (2019) 51–57

Contents lists available at ScienceDirect

Journal of Organometallic Chemistry

journal homepage: www.elsevier.com/locate/jorganchem

Syntheses, structures and *in vitro* cytostatic activity of four novel homochiral organotin(IV) phosphonates

Bo-Hang An, Ru-Fen Zhang**, Qian-Li Li, Xiu-Mei Du, Jing Ru, Shao-Liang Zhang, Chun-Lin Ma*

Institution of Functional Organic Molecules and Materials, School of Chemistry and Chemical Engineering, Liaocheng University, Liaocheng, 252059, China

ARTICLE INFO

Article history:
Received 9 October 2018
Received in revised form
3 December 2018
Accepted 4 December 2018
Available online 5 December 2018

Keywords:
Organotin (IV)
Phosphonates
Syntheses
Structures characterize
Cytostatic activity

ABSTRACT

Four novel homochiral organotin phosphonates, namely, (R)-, (S)-$[(Me_3Sn)_2(pemp)(H_2O)]_n$ (**1**, **2**) and (R)-, (S)-$[(Ph_3Sn)_2(pemp)_2]_n$ (**3**, **4**) [$pempH_2$ = (R)- or (S)-(1-phenylethylamino) methylphosphonic acid], were synthesized and characterized by X-ray diffraction analysis, elemental analysis, FT-IR, NMR (^1H, ^{13}C, ^{31}P and ^{119}Sn), TGA (thermogravimetric analysis) and CD (circular dichroism spectra). The structure analysis indicates that complex **1** displays 1D left-handed helical chain and complex **2** shows right-handed helical chain. These 1D chains are further linked into a 2D supramolecular network architecture through the intermolecular O—H···O interactions. Complexes **3** and **4** are isostructural that showing 1D infinite zig-zag chain structure. In addition, the molecules of complexes **3** and **4** are further linked through intermolecular C—H···π interactions into a 2D supramolecular structure. Furthermore, we preliminarily estimated *in vitro* cytostatic activity of complexes **1**—**4** against the human cervix tumor cells (HeLa) and the human hepatocellular carcinoma cells (HepG-2).

1. Introduction

Phosphonyl derivatives have aroused a great interest because of their potential biological properties as insecticides, fungicides, antiviral agents, and enzyme inhibitors [1–5]. Among these, aminophosphonic acids and their esters, as structural mimics of natural amino acids, have been extensively investigated. As a consequence, aminophosphonic acid derivatives have exhibited a broad range of biological activities as bacterial/viral/fungal infection, neurotransmission and cardiovascular misfunction [6–8]. Recent researches have further extended their applications as anticancer and antituberculosis agents [6,9]. Furthermore, chiral effects appear in a wide variety of natural phenomena. Chiral coordination polymers have aroused intense current interest mainly because of their potential applications in the areas of medicine, catalysis, materials science and other fields [10–15]. Thus, chiral aminophosphorus derivatives are significant compounds in organic and medicinal chemistry [16].

Meanwhile, the organotin compounds are attracting more and more attention owing to their structural diversity and their potential biological activities [17,18]. Between the broad ranges of biological activity, it is worth that mentioning organotin complexes have shown potent *in vivo* and *in vitro* antitumor activities and appeared as biologically active metallopharmaceuticals [19–21]. Further, organotin carboxylates, an important class of compounds with structural diversity ranging from monomeric, dimeric, tetrameric to polymeric motifs [22–24], have been extensively studied owing to their fascinating biological activity and broad applications in catalysis, organic synthesis, material chemistry, medicine and agriculture [25–30]. Thus, in the past few decades, a large amount of work on the synthesis and *in vitro* cytostatic activity of organotin carboxylates have been reported [31–33]. Comparing with the carboxylate group, the phosphonate group contains three potential coordinating oxygen atoms, which may possess the versatile coordination modes and strong coordination capabilities, so they result in a number of metal phosphonates with abundant structural types and interesting properties. Metal phosphonates as a class of important metal–organic frameworks (MOFs) possess a variety of potential applications in ion exchange and adsorption, catalysis, and proton conductivity [34–39]. Although recently the coordination chemistry of organotin phosphonates has been studied to some extent, the reports include various structural types such as monomer, polymer and macrocyclic structures [40–43].

* Corresponding author.
** Corresponding author.
E-mail addresses: zhangrf856@163.com (R.-F. Zhang), macl856@163.com (C.-L. Ma).

https://doi.org/10.1016/j.jorganchem.2018.12.004
0022-328X/

Nevertheless, to our knowledge, little work has been reported on the antitumor activity of organotin phosphonates. It is well known that structural diversity can significantly affect their biological properties [44]. Thus, preparing and exploring the interesting biological activities of organotin phosphonates have become a significant research.

Based on the above background, we were encouraged to select the homochair aminophosphonic acids as the ligands to design and synthesize novel organotin phosphonate derivatives for further biological assessment and interesting structures. Accordingly, we investigated the reactions of Me_3SnCl and Ph_3SnCl with (R)- or (S)-(1-phenylethylamino) methylphosphonic acid and successfully obtained four novel homochiral organotin phosphonate derivatives to farther estimate *in vitro* antitumor activity against the cervix tumor cells (HeLa) and the human hepatocellular carcinoma cells (HepG-2). Intriguingly, the deprotonated phosphonic acid ligands adopt a tridentate coordination mode [Scheme 1 (A)] for the resulting organotin phosphonates based on trimethyltin, while the ligands adopt a bidentate coordination mode [Scheme 1 (B)] for the organotin phosphonates based on triphenyltin. Further, the trimethyltin phosphonates present 1D left-handed helical chain or 1D right-handed helical chain, while the triphenyltin phosphonates show 1D infinite zig-zag chain structure. More attractively, the triphenyltin phosphonates show the higher cytostatic activity than the trimethyltin phosphonates against HeLa cell lines or HepG-2 cell lines. Herein, we detailed the synthesis, structures and *in vitro* cytostatic activity of four novel homochiral organotin phosphonates.

2. Results and discussion

2.1. IR spectra

The IR spectra of complexes **1**–**4** reveal sharp peaks in the 990–1200 cm^{-1} region, which are attributed to the stretching vibrations of the $-PO_3^{2-}$ group. The strong absorptions at 450–490 cm^{-1} and 510–560 cm^{-1} in the spectra of complexes **1**–**4**, which are absent in the spectrum of the ligands, are attributed to Sn–O and Sn–C stretching vibration modes, respectively. For complexes **1** and **2**, the absorption observed at 3305 cm^{-1} is derived from the presence of protons on the water molecule (Fig. S1). The conclusions are consistent well with the X-ray crystallography study.

2.2. NMR spectra

The ^1H NMR spectra of all the complexes show that the signal for the –OH proton (11.98 ppm) in the spectrum is absent compared with the ligand ^1H NMR spectrum, indicating the removal of the –OH proton and the formation of the phosphonate group. Methyl protons (Sn–CH_3 moiety) of complexes **1** and **2** show triplets at 0.34 and 0.39 ppm respectively, along with the coupling constant ^2J (^{119}Sn-^1H) (72 Hz for **1** and 68 Hz for **2**). These values normally correspond to pentacoordinated tin, $\theta = 121.8°$ (**1**) and 118.1° (**2**), respectively [45].

The ^{13}C NMR spectra of complexes **1** and **2** show that complexes present sharp signals at 1.71 and −2.56 ppm with the ^1J (^{119}Sn-^{13}C) value of 503 and 499 Hz, respectively. The magnitude of tin-carbon J coupling, $|^1J(^{119}Sn\text{-}^{13}C)|$, depends linearly on the C-Sn-C angle for a number of tetra-, penta-, and hexacoordinated trimethyltin complexes. $|^1J(^{119}Sn\text{-}^{13}C)| = 11.4\ \theta$ - 875 (where θ = the Me-Sn-Me angle) ($|^1J(^{119}Sn\text{-}^{13}C)|$ is measured in Hz) [45,46]. Such, the C–Sn–C angle were 120.8° (**1**) and 120.5° (**2**). As a result, the tin atoms in complexes **1** and **2** show distorted trigonal bipyramidal geometry. The conclusions drawn are consistent well with the X-ray crystallography study.

The ^{31}P NMR spectra of complexes **1**–**4** show one resonances at 14.04, 16.30, 11.51 and 11.87 ppm, respectively.

The ^{119}Sn NMR spectra of complexes **1** and **2** present signals at 24.92 and 29.65 ppm respectively, which are typical of a four-coordinated tin atom [47]. But this conclusion is different from the result of X-ray crystallography study. Complexes **1** and **2** change their geometry in solution probably by the dissociation of certain weak O→Sn coordinate bond. This can be attributed to the electron donating nature of the Sn-attached alkyl groups that enhanced electronic density on tin atoms and lower down its affinity for O, which is quite common in the organotin(IV) phosphonates [48]. We cannot obtain satisfactory ^{119}Sn NMR spectra for the complexes **3** and **4** because they are poorly soluble in conventional deuterium reagents.

2.3. CD spectra

It is worth mentioning that the enantiomeric nature of complexes **1**–**4** is confirmed by CD spectra which exhibit mirrored responses with Cotton effects of opposite signs. As shown in Fig. 1 (a), positive Cotton effects of complex **1** are evident at 206.5 and 219.1 nm, and negative dichroic signals are centered at 263.4 nm, while **2** exhibits the opposite sign of Cotton effects at the same wavelength. Complexes **3** and **4** exhibit mirror dichroic signals at 206.5, 216.2, 227.3, 234.6 and 258.4 nm [Fig. 2 (b)].

Further, the signals of Cotton effects for complexes **1**–**4** appear below 300 nm, demonstrating that the chirality of the complexes stems from the chiral phosphonate ligand. The lack of CD signals in the visible region suggests that the chiral transformation from the ligand to the whole structure is not evident [49].

2.4. Description of crystal structures

2.4.1. Crystal structures of complexes *1* and *2*

Single-crystal structural determinations reveal that complexes **1** and **2** are enantiomers crystallize in the monoclinic system, chiral space group *P2(1)*. Thus, only the crystal structure of complex **1** is described in detail. The asymmetric unit of complex **1** contains two Me_3Sn units, one deprotonated R-pempH_2, and one coordinating water molecule, as shown in Fig. 2 (a). Center Sn(1) atom is situated in a distorted pentacoordinated trigonal bipyramidal geometry ($\tau = 0.75$; cf. the τ values for the idealized geometries are $\tau = 0$, rectangular pyramidal; $\tau = 1$, trigonal bipyramidal) [50]. The equatorial plane of the trigonal bipyramid geometry is defined by three carbon atoms from Me_3Sn [the sum of the trigonal C–Sn(1)–C angles is 360°], and the axial position is occupied by two oxygen atoms from the bridging ligand [axial angle: O(2)#1–Sn(1)–O(1) 170.12(2)° (#1: 1-x, 0.5 + y, -z)]. Center Sn(2) atom is also situated in a distorted pentacoordinated trigonal bipyramidal geometry ($\tau = 0.94$). The equatorial plane of the trigonal bipyramid is defined by three carbon atoms from Me_3Sn and the axial position is derived from one oxygen atom of bridging ligands and another oxygen atom from coordinating water molecule. The sum of angles subtended at the Sn(2) atom [C(15)–Sn(2)–C(14) 119.5(6)°; C(14)–Sn(2)–C(13) 116.9(6)°; C(15)–Sn(2)–C(13) 120.8(6)°] is close to

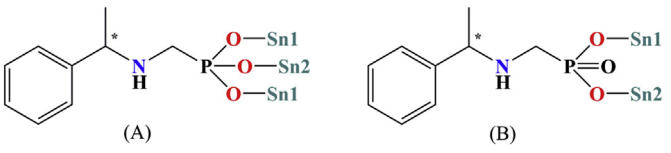

Scheme 1. Various coordination modes of the deprotonated ligand.

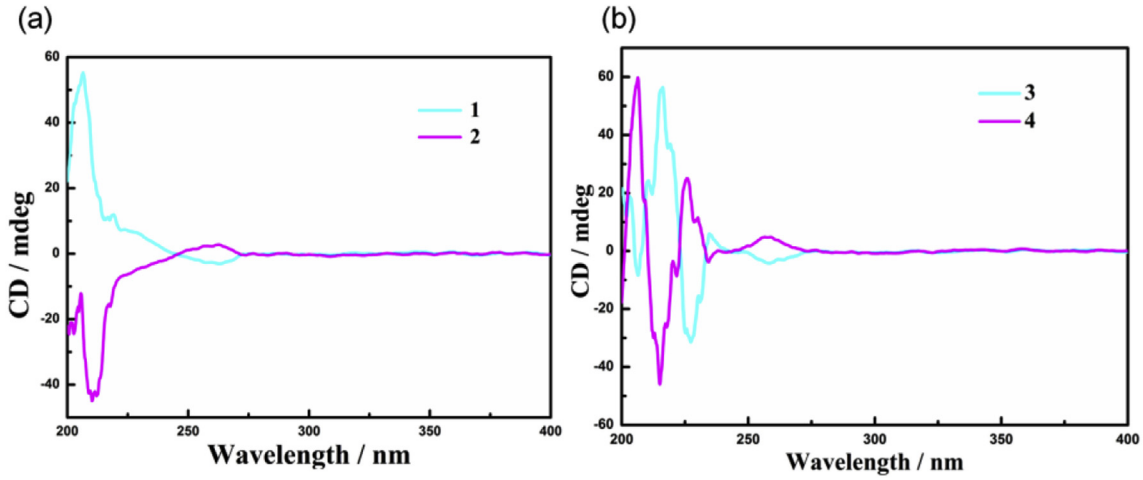

Fig. 1. Solution circular dichroism spectra for complexes **1** and **2** (a), **3** and **4** (b).

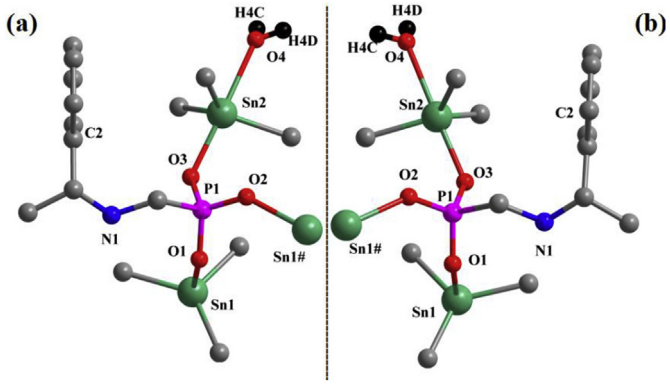

Fig. 2. Asymmetric units of structures **1** (a) and **2** (b). All hydrogen atoms are omitted for clarity.

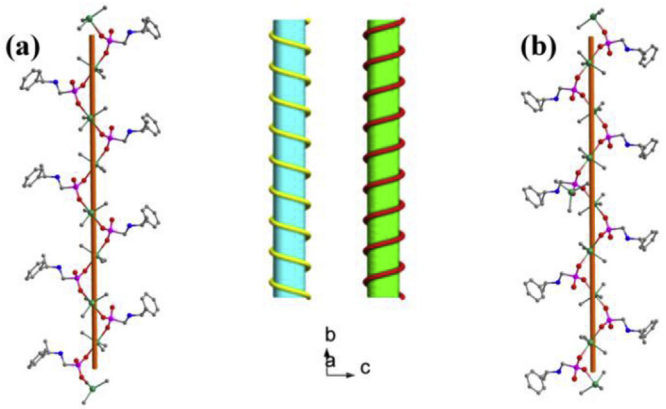

Fig. 3. A helical chain running of complexes **1** (a) and **2** (b). All hydrogen atoms are omitted for clarity.

360°, indicating that Sn(2) and three carbon atoms are occupied an equatorial plane. The corresponding axial–Sn–axial angle [O(3)–Sn(2)–O(4) 177.0(3)°] is close to 180°. The Sn–O distances [Sn(1)–O(1) 2.295(6) Å, Sn(1)–O(2)#1 2.217(7) Å, Sn(2)–O(3) 2.125(5) Å, Sn(2)–O(4) 2.484(6) Å] are between the covalent bond length (2.13 Å) and the van der Waals radii (3.69 Å), which verified that it contained strong covalent bond between the tin atoms and oxygen atoms.

As for deprotonated R-pempH$_2$ ligands, they adopt a tridentate coordination mode. The two adjacent ligands are linked by tin atoms, which alternately afford a 1D left-handed helical chain [Fig. 3 (a)]. Furthermore, these 1D left-handed chains are linked into a 2D supramolecular network architecture through the intermolecular O4–H4C···O1 and O4–H4D···O1 [Distances: O4–H4C···O1 2.385 Å, O4–H4D···O1 2.375 Å. Angles: O4–H4C–O1 120.42°, O4–H4C–O1 121.27°] interactions (Fig. 4), in which 18-membered tetranuclear macrocyclic rings constituted four Me$_3$Sn units, four deprotonated R-pempH$_2$ ligands and two coordinating water molecules, as shown in Fig. 4 (b).

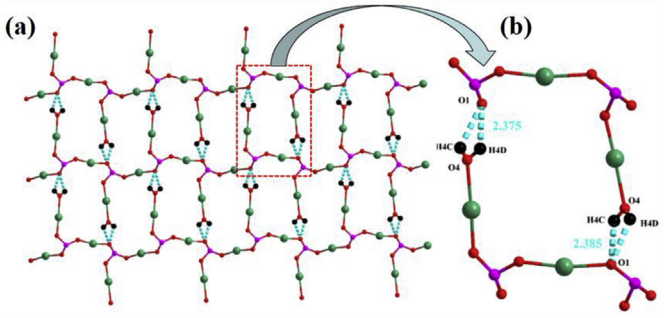

Fig. 4. The 2D network of complex **1**. Some ligands C and H atoms are omitted for clarity.

*2.4.2. Crystal structures of complexes **3** and **4***

Complexes **3** and **4** are enantiomers, so we select complex **3** as an example to describe the details of the structures. Complex **3** crystallizes in the orthorhombic system, chiral space group *P*2(1)2(1)2(1). The asymmetric unit contains two Ph$_3$Sn units and two deprotonated R-pempH$_2$, as shown in Fig. 5 (a). The coordination environment of Sn(1) and Sn(2) atoms are the equivalents. So we select the Sn(1) atom as an example to describe the details of geometry. Center Sn(1) atom adopts distorted five-coordinated trigonal bipyramidal geometry ($\tau = 0.79$). The equatorial plane of the trigonal bipyramid is defined by three carbon atoms from Ph$_3$Sn and the axial position is derived two O atoms from two symmetry related bridging ligands. The sum of angles subtended at the Sn atom [C(16)–Sn(1)–C(22) 112.8(3)°, C(16)–Sn(1)–C(10) 129.2(3)°, C(22)–Sn(1)–C(10) 117.9(3)°] is close to 360°, indicating that Sn

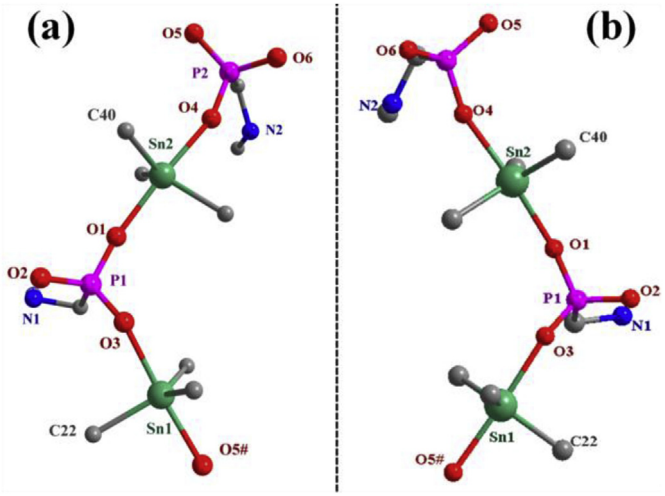

Fig. 5. The asymmetric units of structures **3** (a) and **4** (b). Some carbon atoms are omitted for clarity.

and three carbon atoms are occupied an equatorial plane. The corresponding axial–Sn–axial angle [O(3)–Sn(1)–O(5)#1176.3(2)° (#1: x-1, y, z)] is close to 180°. The Sn–O distances [Sn(1)–O(3) 2.205(6) Å, Sn(1)–O(5)#1 2.203(5) Å] are between the covalent bond length (2.13 Å) and the van der Waals radii (3.69 Å), which proves that the Sn atoms are in coordination with the O atoms by strong covalent bonds.

The deprotonated R-pempH$_2$ symmetrically bridges two Sn atoms by bidentate coordination mode, which leads to a 1D infinite zig-zag chain structure as shown in the view of Fig. 6 (a). Furthermore, complex **3** is further linked through intermolecular C–H···π (C8–H8B···centroid = 2.726 Å) interactions into a 2D supramolecular network structure [Fig. 6 (b)].

2.5. TGA studies

Thermogravimetric analysis (TGA) were carried out under a nitrogen atmosphere to further demonstrate the thermal stability of complexes **1**–**4**, shown in Fig. S2. The TGA data of complexes **1** and **2** show that a first major weight loss equal to 3.41% (**1**), 3.44% (**2**) were seen in the range of 64.69–104.67 °C, ascribing to the loss of one coordinating water (calculated: 3.22%). Such, the conclusions drawn from the TGA data are consistent well with the IR and X-ray crystallography study. As the temperature increased, a noticeable weight loss of complexes **1**–**4** was observed from 176 °C, which indicated the decomposition of the whole structure. The results of the TGA for complexes **1**–**4** indicate high thermal stability (Fig. S2).

2.6. Antitumor activity studies

The *in vitro* cytotoxic activity of the organotin phosphonates **1**–**4** against two tumor human cells, HeLa (the human cervix tumor cells) and HepG-2 (the human hepatocellular carcinoma cells) have been evaluated preliminarily by means of the MTT assays. And the IC_{50} (μmol/L) values, calculated from the dose survival curves, are obtained after 24 h of drug treatment in the MTT test. The half inhibition rates (IC_{50} value) for complexes **1**–**4** are summarized in Table 1. As a comparison, ligands were also tested for cytotoxicity against the two cells, shown in Table 1.

As shown in Table 1, the IC_{50} values of complexes with trimethyl (**1** and **2**) against HeLa cells are 32.286 μmol/L (**1**), 34.439 μmol/L (**2**), respectively. Whereas the IC_{50} values of complexes with triphenyl (**3** and **4**) against HeLa cells are both <0.01 μmol/L. Meanwhile, the IC_{50} values of R and S-ligands against HeLa cells are both >100 μmol/L. Based on the above data analysis, We could summarize as follows: (1) The organotin phosphonates **1**–**4** show higher activity than R or S-ligands against the HeLa cells according to the acquired data; (2) The complexes with phenyl (**3** and **4**) show the higher activity than the methyl (**1** and **2**) against HeLa cells. This is presumably attributed to the presence of phenyl groups showing higher lipophilic character than the methyl groups, which facilitate binding to biological molecules. The similar results are also found in the organotin carboxylate complexes, such as $Ph_3Sn(O_2CC_6H_4$-SO_2NH_2-4) with the IC_{50} value of 0.4 μmol/L shows higher activity than $Me_3Sn(O_2CC_6H_4$-SO_2NH_2-4) with the IC_{50} value of 75.3 μmol/L against HeLa cells [51]. Meanwhile, the complexes (**1** and **2**) contain coordinating water that makes lipophilicity greatly reduced [52].

Table 1
IC_{50} of complexes **1**–**4** and **ligands** against HeLa and HepG-2 cells.

Complex	IC_{50} (μmol/L)		
	HeLa	HepG-2	Ref.
1	32.286	>100	a
2	34.439	>100	a
3	<0.01	2.654	a
4	<0.01	4.420	a
R-ligand	>100	>100	a
S-ligand	>100	>100	a

[a]this work; R = (R) - (1-phenylethylamino) methylphosphonate; S = (S)-(1-phenylethylamino) methylphosphonate.

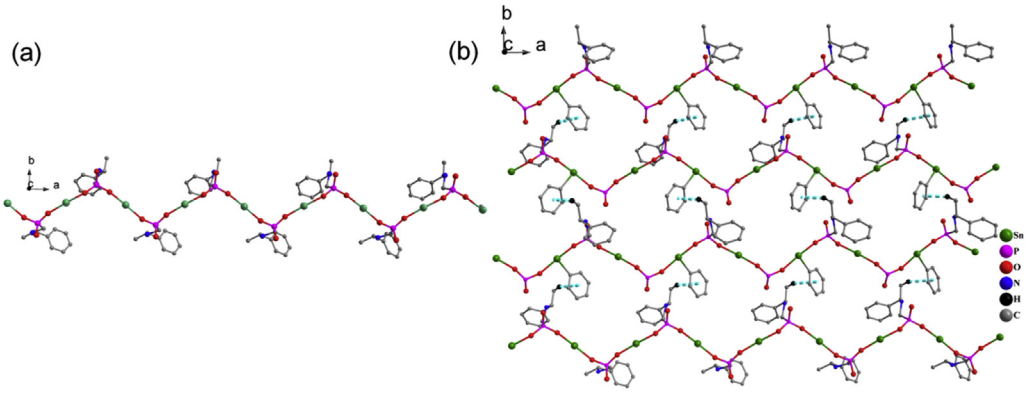

Fig. 6. (a) 1D zig-zag chain; (b) 2D network of complex **2**. Some C atoms are omitted for clarity.

Furthermore, we summarized the same conclusion by preliminary estimating *in vitro* cytostatic activity of the complexes **1**–**4** and ligands against HepG-2 cells. The similar results are also found in the organotin carboxylate complexes, such as $Ph_3Sn(O_2CC_6H_4$-SO_2NH_2-4) with the IC_{50} value of 5.2 μmol/L shows higher activity than $Me_3Sn(O_2CC_6H_4$-SO_2NH_2-4) with the IC_{50} value of >100 μmol/L against HepG-2 cells [51].

On the other hand, from experimental data, we observe that the organotin phosphonates **1**–**4** show different activity against HeLa cells and HepG-2 cells. For instance, the organotin phosphonate **4** with the IC_{50} value of <0.01 μmol/L against HeLa cells shows higher activity than against the HepG-2 cells with the IC_{50} value of 4.420 μmol/L. This is presumably attributed to different inhibitory effects on different cancer cells for the same complex. As the experimental results are preliminary, further research on the antitumor mechanisms of these complexes is ongoing.

3. Conclusions

In summary, we have synthesized and characterized four homochiral organotin phosphonates based on (S) - or (R)-(1-phenylethylamino) methylphosphonic acid. The center tin atoms of the complexes **1**–**4** adopt distorted five-coordinated trigonal bipyramidal geometry. Furthermore, the complex **1** displays 1D left-handed helical chain and complex **2** shows right-handed helical chain. Complexes **3** and **4** are isostructural, showing 1D infinite zig-zag chain structure. Most remarkably, preliminary *in vitro* cytotoxic assessments of complexes **1**–**4** against HeLa and HepG-2 cell lines demonstrate that triphenyl organotin phosphonates (**3** and **4**) exhibit higher activity than the trimethyl complexes (**1** and **2**). This result enriches the possibility of designing novel anticancer metal-based drugs.

4. Experimental section

4.1. Physical measurements

The melting points were obtained with a Kofler micro-melting point apparatus and were uncorrected. Elemental analysis were performed with a PE-2400II apparatus. Infrared spectra were recorded with a Nicolet-5700 spectrometer using KBr discs. ^1H, ^{13}C, ^{31}P, and ^{119}Sn NMR spectra were recorded with a Varian Mercury Plus 400 spectrometer operating at 400, 100, 162 and 149 MHz, respectively. The spectra were acquired at room temperature (298 K). ^{13}C NMR spectra were broadband-proton-decoupled. The chemical shifts were reported in ppm with respect to the references and were stated relative to external tetramethylsilane (TMS) for ^1H, ^{13}C, ^{31}P, and ^{119}Sn NMR. Thermogravimetric analysis (TGA) were performed on a V5.1A Dupont 2100 instrument from room temperature to 800 °C with a heating rate of 20 K min^{-1} under flowing nitrogen. Assays were conducted using 96-well microplates. The solution circular dichroism spectra were recorded on a JASCO-810 spectropolarimeter using methanol solvent at room temperature.

4.2. Materials and synthesis

(S)- or (R)-(1-phenylethylamino) methylphosphonic acid was prepared by reactions of (S)- and (R)-1-phenylethylamine, diethyl phosphite, and paraformaldehyde, according to literature methods [49]. (S)- and (R)-1-phenylethylamine were purchased from Energy Chemical without further purification, and all of the other starting materials were of reagentgrade quality.

The synthesis procedures of complexes are given in Scheme 2. As shown in Scheme 2, a 1:2:2 ration of $pempH_2$, sodium ethoxide and trimethyltin chloride in methanol afford organotin ester: $[(Me_3Sn)_2(pemp)(H_2O)]_n$ (**1**, **2**); A 1:2:2 ration of $pempH_2$, sodium ethoxide and triphenyltin chloride in methanol afford organotin ester: $[(Ph_3Sn)_2(pemp)_2]_n$ (**3**, **4**).

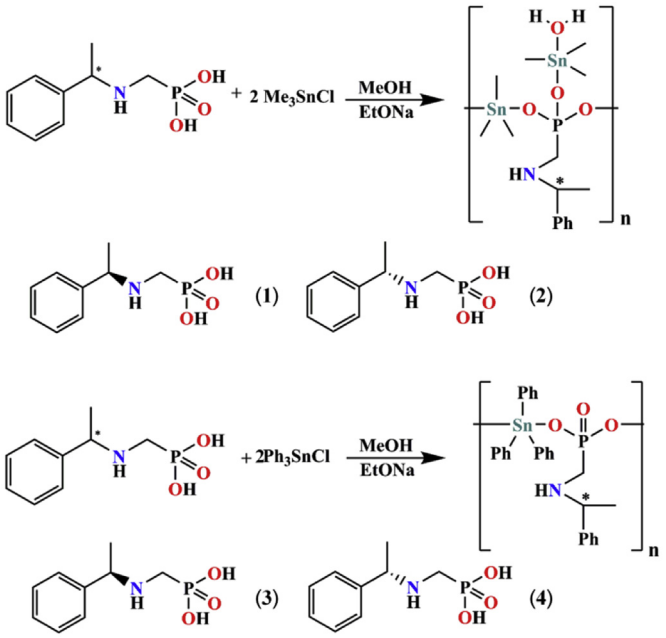

Scheme 2. The synthetic procedures of obtained complexes.

4.2.1. (R)-$[(Me_3Sn)_2(pemp)(H_2O)]_n$ (1)

A mixture of R-$pempH_2$ (107.5 mg, 0.5 mmol), sodium ethoxide (68.0 mg, 1.0 mmol) in methanol (30 ml) was stirred for 30 min, followed by the addition of trimethyltin chloride (199.0 mg, 1.0 mmol) and further stirred for 12 h at 55 °C. The solvent was gradually removed by evaporation under reduced pressure until a solid product was obtained. The powder was then recrystallized from the ether, and transparent colorless crystals were recovered. Yield: 154.2 mg, 55.2%. M.P.: 95 °C. Anal. Calc. for $C_{15}H_{32}NO_4PSn_2$: C 32.24; H 5.77; N 2.51%. Found: C 31.86; H 5.63; N 2.48%. IR (KBr, cm^{-1}): 3445, 3305, 3062, 2962, 2925, 1687, 1493, 1465, 1374, 1345, 1129, 1106, 1062, 1018, 994, 552, 489. ^1H NMR [$(CD_3)_2SO$, 400 MHz, ppm]: $\delta = 0.34$ (t, Sn−CH_3, $^2J_{Sn\text{-}H} = 72$ Hz); 1.20 (d, −CH_3, $^3J_{H\text{-}H} = 8$ Hz); 2.10 (d, N−CH_2−P, $J_{H\text{-}H} = 12$ Hz); 3.67 (brs, −C_6H_5−CH−N); 7.16–7.27 (m, −C_6H_5). ^{13}C NMR ($CDCl_3$, 100 MHz, ppm): $\delta = 130.68$–146.94 (−C_6H_5); 62.91 (C_6H_5−CH−N); 48.83 (N−CH_2−P); 25.50 (−CH_3); 1.71 (Sn−CH_3, $^1J_{Sn-C} = 503$ Hz). ^{31}P NMR ($CDCl_3$, 162 MHz, ppm): $\delta = 14.04$. ^{119}Sn NMR ($CDCl_3$, 149 MHz, ppm): $\delta = 24.92$.

4.2.2. (S)-$[(Me_3Sn)_2(pemp)(H_2O)]_n$ (2)

Complex **2** was obtained similarly except that S-$pempH_2$ was used. Yield: 156.7 mg, 56.1%. M.P.: 97 °C. Anal. Calc. for $C_{15}H_{32}NO_4PSn_2$: C 32.24; H 5.77; N 2.50%. Found: C 32.14; H 5.71; N 2.49%. IR (KBr, cm^{-1}): 3442, 3305, 3062, 2962, 2925, 1688, 1493, 1465, 1374, 1345, 1129, 1105, 1061, 1018, 994, 552, 489. ^1H NMR [$(CD_3)_2SO$, 400 MHz, ppm]: $\delta = 0.39$ (t, Sn−CH_3, $^2J_{Sn\text{-}H} = 68$ Hz); 1.25 (d, −CH_3, $^3J_{H\text{-}H} = 8$ Hz); 2.26 (d, N−CH_2−P, $^3J_{H\text{-}H} = 16$ Hz); 3.70, 3.72 (dd, C_6H_5−CH−N, $^3J_{H\text{-}H} = 16$ Hz); 7.14–7.25 (m, −C_6H_5). ^{13}C NMR (CD_3OD, 100 MHz, ppm): $\delta = 126.79$–142.38 (−C_6H_5); 58.99 (C_6H_5−CH−N); 46.12 (N−CH_2−P); 21.17 (−CH_3); −2.56 (Sn−CH_3, $^1J_{Sn-C} = 499$ Hz). ^{31}P NMR ($CDCl_3$, 162 MHz, ppm): $\delta = 16.30$. ^{119}Sn NMR ($CDCl_3$, 149 MHz, ppm): $\delta = 29.65$.

Table 2
Crystallographic data and structure refinement parameters for complexes **1**, **2**, **3** and **4**.

Complex	1	2	3	4
Empirical formula	$C_{15}H_{32}NO_4PSn_2$	$C_{15}H_{32}NO_4PSn_2$	$C_{54}H_{54}N_2O_6P_2Sn_2$	$C_{54}H_{54}N_2O_6P_2Sn_2$
M	558.77	558.77	1126.31	1126.31
Crystal system	Monoclinic	Monoclinic	Orthorhombic	Orthorhombic
space group	*P2(1)*	*P2(1)*	*P2(1)2(1)2(1)*	*P2(1)2(1)2(1)*
a [Å]	9.2743(7)	9.2427(7)	12.1292(11)	12.1821(11)
b [Å]	10.9557(8)	10.9281(8)	17.1333(15)	17.2319(16)
c [Å]	11.7163(9)	11.6746(9)	23.791(2)	23.930(2)
α [°]	90	90	90	90
β [°]	92.690(2)	92.689 (1)	90	90
γ [°]	90	90	90	90
V [Å^3]	1189.14(15)	1177.90(15)	4944.1(8)	5023.3(8)
Z	2	2	4	4
D_{calc} (Mg/m^3)	1.561	1.575	1.513	1.489
M (mm^{-1})	2.182	2.203	1.127	1.109
F (000)	552	552	2280	2280
Crystal size(mm)	0.39 × 0.20 x 0.10	0.38 × 0.27 x 0.14	0.23 × 0.21 x 0.11	0.16 × 0.14 x 0.03
Reflections collected	5860	5892	24408	24942
Unique reflections	3999	3834	8722	8829
R (int)	0.0316	0.0242	0.0415	0.1005
Goodness-of-fit on F^2	0.949	1.072	0.771	0.802
Final R indices[$I>2$sigma(I)]	R_1[a] = 0.0363, wR_2[b] = 0.0760	R_1[a] = 0.0293, wR_2[b] = 0.0580	R_1[a] = 0.0349, wR_2[b] = 0.0764	R_1[a] = 0.0488, wR_2[b] = 0.1116
R indices (all data)	R_1[a] = 0.0442, wR_2[b] = 0.0797	R_1[a] = 0.0393, wR_2[b] = 0.0630	R_1[a] = 0.0560, wR_2[b] = 0.0926	R_1[a] = 0.0702, wR_2[b] = 0.1239

[a] $R_1 = \sum||F_o| - |F_c||/\sum|F_o|$.
[b] $wR_2 = \{\sum[w(F_o^2 - F_c^2)2]/\sum[w(F_o^2)^2]\}^{1/2}$.

4.2.3. (R)-[(Ph$_3$Sn)$_2$(pemp)$_2$]$_n$ (3)

A mixture of R-pempH$_2$ (107.5 mg, 0.5 mmol), sodium ethoxide (68.0 mg, 1.0 mmol) in dry methanol (30 ml) was stirred for 30 min, followed by the addition of triphenyltin chloride (385.5 mg, 1.0 mmol) and further stirred for 12 h at 50 °C. The solvent was gradually removed by evaporation under reduced pressure until a solid product was obtained. The powder was then recrystallized from the methanol, and transparent colorless crystals were recovered. Yield: 272.0 mg, 48.3%. M.P.: >300 °C. Anal. Calc. for $C_{54}H_{54}N_2O_6P_2Sn_2$: C 57.58; H 4.83; N 2.49%. Found: C 57.23; H 4.63; N 2.36%. IR (KBr, cm^{-1}): 3421, 3051, 2985, 2965, 1591, 1496, 1481, 1455, 1374, 1331, 1079, 1057, 997, 514, 456. ^{1}H NMR [(CD$_3$)$_2$SO, 400 MHz, ppm]: δ = 0.91 (s, −C*H*$_3$); 2.14 (brs, N−C*H*$_2$−P); 3.68 (brs, −C$_6$H$_5$−C*H*−N); 7.16–7.96 (m, C$_6$*H*$_5$). ^{13}C NMR [(CD$_3$)$_2$SO, 100 MHz, ppm]: δ = 127.89–137.16 (−C$_6$H$_5$); 58.98 (C$_6$H$_5$−*C*H−N); 40.63 (N−*C*H$_2$−P). ^{31}P NMR [(CD$_3$)$_2$SO, 162 MHz, ppm]: δ = 11.51.

4.2.4. (S)-[(Ph$_3$Sn)$_2$(pemp)$_2$]$_n$ (4)

Complex **4** was obtained similarly except that S-pempH$_2$ was used. Yield: 268.1 mg, 47.6%. M.P.: >300 °C. Anal. Calc. for $C_{54}H_{54}N_2O_6P_2Sn_2$: C 57.58; H 4.83; N 2.49%. Found: C 57.33; H 4.70; N 2.38%. IR (KBr, cm^{-1}): 3420, 3051, 2984, 2965, 1958, 1889, 1819, 1591, 1496, 1481, 1455, 1374, 1331, 1079, 952, 514, 456. ^{1}H NMR [(CD$_3$)$_2$SO, 400 MHz, ppm]: δ = 0.88 (s, −C*H*$_3$); 2.11 (brs, N−C*H*$_2$−P); 3.65 (brs, −C$_6$H$_5$−C*H*−N); 7.13–7.96 (m, −C$_6$*H*$_5$). ^{13}C NMR [(CD$_3$)$_2$SO, 100 MHz, ppm]: δ = 127.86–137.20 (−C$_6$H$_5$); 59.07 (C$_6$H$_5$−*C*H−N); 40.63 (N−*C*H$_2$−P). ^{31}P NMR [(CD$_3$)$_2$SO, 162 MHz, ppm]: δ = 11.87.

4.3. X-ray crystallography

Data collections for complexes were carried out on a Bruker SMART-1000 CCD diffractometer equipped with graphite monochromated Mo-Kα (λ = 0.71073 Å) radiation at room temperature. The data were integrated and corrected for Lorentz and polarization effects using SAINT [53]. Absorption corrections were applied with SADABS [54]. The structures were solved by the direct method and refined by full-matrix least squares method on F^2 using the SHELXTL crystallographic software package [55]. All the non-hydrogen atoms were refined anisotropically. Hydrogen atoms of the organic ligands were refined as riding on the corresponding non-hydrogen atoms. Additional details of the data collections and structural refinement parameters were provided in Table 2. Selected bond lengths and bond angles of complexes were listed in Tables S1–S4 (Supplementary Material).

4.4. In vitro cytostatic activity assays

The cell viability was determined by MTT dye uptake. The human cervix tumor cells (HeLa) and the human hepatocellular carcinoma cells (HepG-2) were seeded (1 × 10^4 cells per well) into 96-well microtiter plates. RPMI-1640 containing antibiotics (100 μg/mL streptomycin and 100 U penicillin) and 10% fetal bovine serum were used as the culture medium. After 24 h preincubation of the cells in a humidified 5% CO_2 atmosphere at 37 °C, the complexes were added with the concentration of 0.01–10 μmol/L, followed by further incubation for 24 h and the medium was removed and cells were washed using PBS. The MTT solution (5 mg/mL) was added to each well and further incubated for another 4 h, then the supernatant was carefully discarded. Finally, 100 μL DMSO was added to every well, mixed, and measured on a multi-well plate reader (Bio-Rad iMark) at 490 nm.

Acknowledgement

We thank the National Natural Science Foundation of China (21371087) and the Natural Science Foundation of Shandong Province (ZR2017PB014, ZR2018LB003, and ZR2016BB07) for financial support.

Appendix A. Supplementary data

Supplementary data to this article can be found online at https://doi.org/10.1016/j.jorganchem.2018.12.004.

CCDC-1859294 (**1**), 1859295 (**2**), 1859296 (**3**) and 1859297 (**4**) contain the supplementary crystallographic data for this paper. These data can be obtained free of charge via http://www.ccdc.cam.ac.uk/conts/retrieving.html, or from the Cambridge

Crystallographic Data Center, 12 Union Road, Cambridge CB2 1EZ, UK; fax: (+44) 1223-336-033; or e-mail: deposit@ccdc.cam.ac.uk.

References

[1] D. Salvador-Gil, L. Ortego, R.P. Herrera, I. Marzo, M.C. Gimeno, Dalton Trans. 46 (2017) 13745–13755.
[2] C. Phillipj, L. Peterj, S. Maximj, Plant Dis. 93 (2009) 809–814.
[3] J. Huang, R. Chen, Heteroat. Chem. 11 (2000) 480–492.
[4] R. Pauwels, J. Balzarini, D. Schols, M. Baba, J. Desmyter, I. Rosenberg, A. Holy, C.E. De, Antimicrob. Agents Chemother. 32 (1988) 1025–1030.
[5] A. Zhang, Y. Mu, F. Wu, Ecotoxicol. Environ. Saf. 138 (2017) 215–222.
[6] T.E. Ali, S.M. El-Edfawy, Res. Chem. Intermed. 42 (2016) 1329–1347.
[7] B.B. Adhikari, S. Roshandel, A. Fujii, M.P. Schramm, Eur. J. Org Chem. 2015 (2015) 2683–2690.
[8] S. Gress, S. Lemoine, G.-E. Séralini, P.E. Puddu, Cardiovasc. Toxicol. 15 (2015) 117–126.
[9] H.R. Hudson, R.J. Lee, Phosphorus, Sulfur Silicon Relat. Elem. 189 (2014) 1149–1155.
[10] C. Liu, D. Zhang, R. Xiong, X. Hao, D. Zhu, Chem. Commun. 54 (2018) 13379–13382.
[11] S. Lee, E.A. Kapustin, O.M. Yaghi, Science 353 (2016) 808–811.
[12] J. Navarro-Sánchez, A.I. Argente-García, Y. Moliner-Martínez, D. Roca-Sanjuán, D. Antypov, P. Campíns-Falcó, M.J. Rosseinsky, C. Martí-Gastaldo, J. Am. Chem. Soc. 139 (2017) 4294–4297.
[13] Z. Jane Li, D.J.W. Grant, J. Pharmaceut. Sci. 86 (1997) 1073–1078.
[14] G.A. Hembury, V.V. Borovkov, Y. Inoue, Chem. Rev. 108 (2008) 1–73.
[15] M. Yoon, R. Srirambalaji, K. Kim, Chem. Rev. 112 (2012) 1196–1231.
[16] Y. Cao, F. Shen, F. Zhang, J. Zhang, R. Wang, Angew. Chem. Int. Ed. 53 (2014) 1862–1866.
[17] F. Shaheen, M. Sirajuddin, S. Ali, R. Zia ur, P.J. Dyson, N.A. Shah, M.N. Tahir, J. Organomet. Chem. 856 (2018) 13–22.
[18] R. Joshi, N. Pandey, R. Tilak, S.K. Yadav, H. Mishra, S. Pokharia, Appl. Organomet. Chem. 32 (2018) 4324–4339.
[19] N. Gerasimchuk, T. Maher, P. Durham, K.V. Domasevitch, J. Wilking, A. Mokhir, Inorg. Chem. 46 (2007) 7268–7284.
[20] G. Wen, R. Zhang, Q. Li, S. Zhang, J. Ru, J. Du, C. Ma, J. Organomet. Chem. 861 (2018) 151–158.
[21] S. Tabassum, S. Mathur, F. Arjmand, K. Mishra, K. Banerjee, Metallomics 4 (2012) 205–217.
[22] S. Kundu, B. Mohapatra, C. Mohapatra, S. Verma, V. Chandrasekhar, Cryst. Growth Des. 15 (2015) 247–256.
[23] V. Chandrasekhar, R. Thirumoorthi, Organometallics 26 (2007) 5415–5422.
[24] Y.F. Win, S.G. Teoh, M.R. Vikneswaran, S.T. Ha, P. Ibrahim, Chin. J. Chem. 11 (2010) 509–516.
[25] C.O. Kappe, Angew. Chem. Int. Ed. 43 (2004) 6250–6284.
[26] S.T. Handy, X. Zhang, Org. Lett. 3 (2001) 233–236.
[27] A.F. Baldwin, R. Ma, A. Mannodi-Kanakkithodi, T.D. Huan, C. Wang, M. Tefferi, J.E. Marszalek, M. Cakmak, Y. Cao, R. Ramprasad, G.A. Sotzing, Adv. Mater. 27 (2015) 346–351.
[28] N.P. Bharathi, M. Alam, A. TasleemJan, A.A. Hashmi, J. Inorg. Organomet. Polym. 19 (2009) 187–195.
[29] Q. Zhang, X. Hu, M. Wu, Y. Zhao, C. Yu, J. Appl. Polym. Sci. 135 (2018) 46460–46471.
[30] M.H. Sainorudin, N.M. Sidek, N. Ismail, M.Z.H. Rozaini, N.A. Harun, T.N.S.T. Anuar, A.A.A.R. Azmi, F. Yusoff, GSTF J. Chem. Sci. 2 (2013) 10–18.
[31] L. Hu, H. Wang, T. Xia, B. Fang, Y. Shen, Q. Zhang, X. Tian, H. Zhou, J. Wu, Y. Tian, Inorg. Chem. 57 (2018) 6340–6348.
[32] C.S. Rocha, B.P. Morais, B.L. Rodrigues, C.L. Donnici, G.M. Lima, J.D. Ardisson, J.A. Takahashi, R.S. Bitzer, Appl. Organomet. Chem. 31 (2017) 3645–3653.
[33] Y. Zhang, R. Zhang, S. Zhang, S. Cheng, Q. Li, C. Ma, Dalton Trans. 45 (2016) 8412–8421.
[34] J. Huang, H. Ding, Y. Xu, D. Zeng, H. Zhu, D. Zang, S. Bao, Y. Ma, L. Zheng, Nat. Commun. 8 (2017) 2131–2143.
[35] S.S. Bao, G.K.H. Shimizu, L. Zheng, Coord. Chem. Rev. 378 (2019) 577–594.
[36] R. Silbernagel, C.H. Martin, A. Clearfield, Inorg. Chem. 55 (2016) 1651–1656.
[37] Z. Cai, S. Bao, X. Wang, Z. Hu, L. Zheng, Inorg. Chem. 55 (2016) 3706–3712.
[38] S. Bao, Y. Wu, N. Li, L. Zheng, Eur. J. Inorg. Chem. (2016) 4476–4482, 2016.
[39] M. Liu, J. Feng, S. Bao, L. Zheng, Chem. Eur J. 23 (2017) 1086–1092.
[40] W. Diallo, L. Diop, K.C. Molloy, M.F. Mahon, L. Plasseraud, Main Group Met. Chem. 37 (2014) 33–37.
[41] H. Perry, J. Zoń, J. Law, A. Clearfield, J. Solid State Chem. 183 (2010) 1165–1173.
[42] C. Ma, M. Yang, R. Zhang, J. Li, Inorg. Chem. Commun. 10 (2007) 1330–1334.
[43] J. Goura, V. Chandrasekhar, Chem. Rev. 115 (2015) 6854–6965.
[44] S. Syed Shoaib Ahmad, A. Muhammad, W. Amir, M.M. Ahmed, N. Tayyaba, S. Salma, R. Gildardo, Mini Rev. Med. Chem. 15 (2015) 406–426.
[45] T.P. Lockhart, W.F. Manders, Inorg. Chem. 25 (1986) 892–895.
[46] M. Sirajuddin, S. Ali, V. McKee, M. Sohail, H. Pasha, Eur. J. Med. Chem. 84 (2014) 343–363.
[47] M. Sirajuddin, S. Ali, V. McKee, S. Zaib, J. Iqbal, RSC Adv. 4 (2014) 57505–57521.
[48] F. Shaheen, M. Sirajuddin, S. Ali, R. Zia ur, P.J. Dyson, N.A. Shah, M.N. Tahir, J. Organomet. Chem. 856 (2018) 13–22.
[49] Y. Xu, S. Bao, X. Huang, L. Zheng, Cryst. Growth Des. 18 (2018) 4045–4053.
[50] A.W. Addison, T.N. Rao, J. Reedijk, J.V. Rijn, G.C. Verschoor, J. Chem. Soc. Dalton Trans. 7 (1984) 1349–1356.
[51] S. Wang, Q. Li, R. Zhang, J. Du, Y. Li, C. Ma, Polyhedron 158 (2019) 15–24.
[52] D.B. Shpakovsky, C.N. Banti, E.M. Mukhatova, Y.A. Gracheva, V.P. Osipova, N.T. Berberova, D.V. Albov, T.A. Antonenko, L.A. Aslanov, E.R. Milaeva, S.K. Hadjikakou, Dalton Trans. 43 (2014) 6880–6890.
[53] Smart & SAINT Software Reference Manuals, Bruker Analytical X-ray Systems, Inc., Madison, WI, 2003. Version 6.45.
[54] G.M. Sheldrick, A. Sadabs, Software for Empirical Absorption Correction, University of Göttingen, Göottingen, Germany, 2002. Version 2.05.
[55] G.M. Sheldrick, SHELXTL Reference Manual, Bruker Analytical X-ray Systems, Inc., Madison, WI, 2000. Version 6.1.